J. Mod. Transport. (2014) 22(1):50–54
DOI 10.1007/s40534-014-0032-4

www.springer.com/40534

Transport properties and microstructure of $La_{0.7}Sr_{0.3}MnO_3$ nanocrystalline thin films grown by polymer-assisted chemical solution deposition

Min Zhang · Li Lv · Zhantao Wei · Xin Sheng Yang · Xin Zhang

Received: 24 October 2013 / Revised: 28 December 2013 / Accepted: 2 January 2014 / Published online: 21 January 2014

Abstract Perovskite-based materials can be widely used in the aerospace and transportation field. Perovskite manganese oxides $La_{0.7}Sr_{0.3}MnO_3$ (LSMO) thin films were grown on $LaAlO_3$ (100) and Si (100) single crystal substrates by the polymer-assisted chemical solution deposition (PACSD) method. Electronic transport behavior, microstructure, and magnetoresistance (MR) of LSMO thin films on different substrates were investigated. The resistance of LSMO films fabricated on $LaAlO_3$ substrates is smaller than that on the Si substrates. The magnetic field reduces resistance of LSMO films both on Si and LAO in the wide temperature region, when the insulator-metal transition temperature shifts to higher temperature. The low-field magnetoresistance of LSMO films on Si in low temperature range at 1 T is larger than that of LSMO films on LAO. However, the MR of LSMO film on LAO films at room-temperature is about 5.17 %. The thin films are smooth and dense with uniform nanocrystal size grain. These results demonstrate that PACSD is an effective technique for producing high quality LSMO films, which is significant to improve the magnetic properties and the application of automotive sensor.

Keywords Polymer-assisted chemical solution deposition (PACSD) · $La_{0.7}Sr_{0.3}MnO_3$ (LSMO) thin films · Transport properties and microstructure

M. Zhang · L. Lv · Z. Wei · X. S. Yang (✉) · X. Zhang
Key Laboratory of Magnetic Levitation Technologies and Maglev Trains, Ministry of Education of China, and Superconductivity and New Energy R&D Center, Southwest Jiaotong University, Chengdu 610031, China
e-mail: xsyang@swjtu.edu.cn

1 Introduction

Perovskite-based functional materials have a wide application prospect due to colossal magnetoresistance (CMR) and magnetic refrigeration effects. They can be used to make the magnetic head, magnetic resistance memory, and motor transducer. The transducer can be used to measure and control current, position, angle etc. Moreover, they can be used in aerospace, automotive industry as magnetic refrigeration material. In recent years, as the developments of anisotropic MR effect and CMR in ferromagnetic/non-magnetic metal multilayer films, the thin film MR sensor has become one of the most active magnetic sensor technologies, which are widely used in mineral exploration, underground drilling, position detection, navigation etc.

CMR materials such as $(La,Ca)MnO_3$, $(La,Sr)MnO_3$, and $(La,Ca,Sr)MnO_3$ have been extensively investigated on polycrystal, single crystal, and thin films [1–3], due to theirs potential applications in devices such as memory devices, magnetic field sensors, infrared detectors, and spin-based devices [4–8].

Shim et al. [9] reported that the maximum low-field magnetoresistance (LFMR) of LSMO film, was 0.68 %, obtained at 300 K in the 450 Oe field region. Liu et al. [10], also obtained that the LFMR of LSMO film on Si (100) substrate were as high as 2.54 % at $H = 0.05$ T and 300 K. Different from the intrinsic double-exchange-type CMR, induced by a strong magnetic field in the tesla range, the LFMR effect is attributed to spin dependent tunneling across the grain boundaries (GBs).

Many techniques have been applied to preparing $La_{0.7}Sr_{0.3}MnO_3$ epitaxial and polycrystalline films on different substrates including pulsed laser deposition (PLD) [11, 12], sputtering [13, 14], metal organic chemical vapor deposition (MOCVD) [15, 16], molecular beam epitaxy

(MBE) [17], chemical solution deposition (CSD) [18] etc. Among these methods, the CSD method has some advantages for the films deposition and growth such as low cost, high stability, and simple process. As for the CSD technique for the preparation of LSMO films, many researches about epitaxy, concentration of precursor solution, annealing, LFMR as well as the GBs on substrates of MgO, $LaAlO_3$, Si, $SrTiO_3$, and GaAs have been reported [18, 19].

In this article, LSMO films were synthesized on $LaAlO_3$ (100) and Si (100) by polymer-assisted chemical solution deposited (PACSD). The smooth and dense films can be fabricated via this method. Preparation and transport properties on $LaAlO_3$ (100) and Si (100) were investigated because silicon is a good candidate for spin injection and the lattice mismatch of LAO is small enough to induce epitaxy. The microstructure, the surface, and the electronic transport behavior and magnetoresistance (MR) properties of LSMO thin films were presented.

2 Experimental

The nanocrystalline thin films of $La_{0.7}Sr_{0.3}MnO_3$ were grown by PACSD method on (100) $LaAlO_3$ and Si (100) single crystal substrates. For preparation of LSMO thin films, Si (1 0 0), and $LaAlO_3$ (1 0 0) single crystal substrates were cleaned. First, analytical reagents $La(NO_3)_3 \cdot 6H_2O$, $Sr(NO_3)_2$ and $Mn(NO_3)_3 \cdot 6H_2O$ were weighed accurately and dissolved in DMF (*N*,*N*-Dimethylformamide) to obtain anhydrous clear solution with a final solution concentration of 0.3 mol/L. Then, Polyvinylpyrrolidone K30 (PVP) was used to increase the viscosity of solution. Deposition of LSMO was carried out by a spin coater at 500 rpm for 10 s, followed by 4,000 rpm for 50 s. After deposition, the wet films were dried at 80 °C for 10 min. Then the films were pyrolized at temperature 200 °C for 10 min and 500 °C for 20 min. The dried films were finally crystallized at 830–870 °C for 1–2 h in air ambience.

The phases were determined by X-ray diffraction using the Philips X-ray diffractometer X'Pert MRD diffractometer (Cu-K α radiation, $\lambda = 1.54$ Å), the microstructures of the films were also observed using field emission scanning electron microscope (FESEM, JSM-7001F), and the transport properties and magnetic properties were measured by Physical Property Measurement System (PPMS, Quantum Design 9 T).

3 Results and discussion

Figure 1 shows the typical θ–2θ X-ray diffraction spectra of LSMO film grown on LAO (100) substrates. Only (100) and (200) peaks are observed without any impurity peaks, indicating highly *c*-axis oriented growth with pseudo-cubic (100) orientation. From the data, the calculated lattice constants are $a = 3.876$ Å for LSMO and $a = 3.796$ Å for LAO. The lattice mismatch between LSMO (100) films and LAO (100) substrates is 2.1 %, which are evaluated via the definition of

$$\frac{a_f - a_s}{a_s} \times 100\ \%. \quad (1)$$

XRD pattern of LSMO film on Si (100) substrate is presented in Fig. 2. All the main diffraction peaks belong to LSMO phase, implying that the LSMO film on Si is of single phase with perovskite structure. It is obviously different from the film fabricated on the single crystal substrates of $LaAlO_3$, which are advantageous for the growth of (l00) orientation films. The film growth on Si (100) substrate resulted polycrystalline with pseudo-cubic orientation due to the large lattice mismatch degree between LSMO (100) films and Si (100) ($a = 0.539$ nm) substrates. Nevertheless, the small mismatch between LSMO (110) and Si (100) was reported to be 1.8 % in [10]. Therefore, LSMO grains grow via a self-textured growth mode and are randomly oriented.

In order to evaluate the quality of LSMO thin films from the PACSD method, the microstructures of the films were also examined. Figure 3 shows the FE-SEM images of LSMO films on LAO and LSMO films on Si, which displays that the films are smooth and have high crystal quality. It is clear from Fig. 3b that the LSMO films on Si consist of nanometer polycrystalline. Typical grain sizes are in the range of 50–70 nm with some cavities, which may be related to the volatilization of organic precursors. This is in agreement with the results in [9]. Comparing the morphology of the LSMO films on Si (Fig. 3a) and LAO (Fig. 3b), we find that the latter seems to have denser microstructure and smaller crystallites size of 15 nm or so. It can be seen that LSMO film on LAO is the columnar structure with a thickness of 400 nm. The bulk of film is

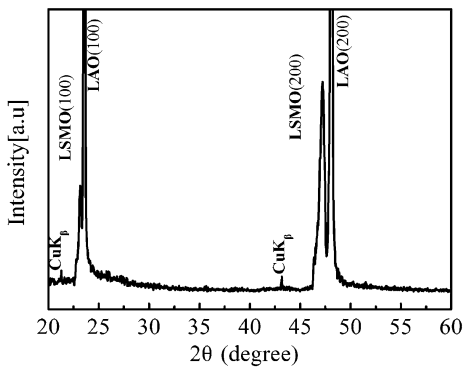

Fig. 1 X-ray diffraction of $La_{0.7}Sr_{0.3}MnO_3$ deposited on LAO (100) substrate

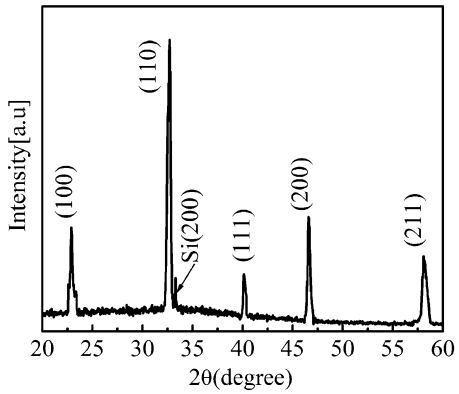

Fig. 2 X-ray diffraction of $La_{0.7}Sr_{0.3}MnO_3$ deposited on Si (100) substrate

epitaxial but the surface exhibits some polycrystalline structure.

These results show that substrate has a significant effect on the crystallographic properties of the resulting thin film.

Figure 4 shows temperature-dependent electrical resistivity ($\rho - T$) for LSMO films on LAO from 360 to 5 K under 0 and 1 T. Note that metal-insulator transition is at 349 K for $H = 0$ T corresponding to bulk samples temperature around 360 K, which proves a good quality of the film. The film exhibits systematic increase in metal-insulator transition temperature (T_{MI}) with an increase of applied magnetic field. Due to limitations of the measurement equipment, insulator-metal transition is not observed in the film under applied magnetic field $H = 1$ T.

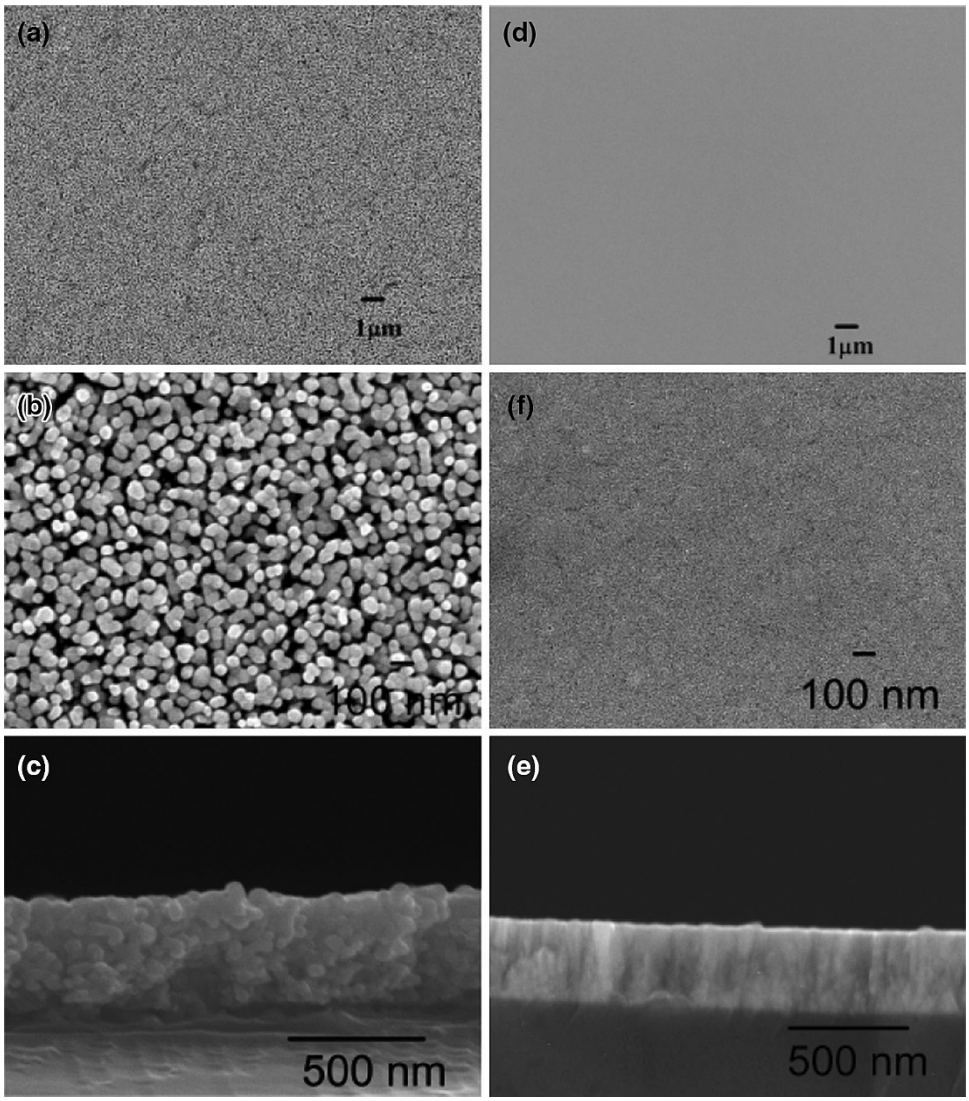

Fig. 3 Typical FE-SEM images for **a** LSMO film on Si and **b** LSMO film on Si collected at ×5,000 and ×50,000 magnification, respectively. **c** The cross-sectional morphology of LSMO film on Si. **d** LSMO film on LAO film and **e** LSMO film on LAO collected at ×5,000 and ×50,000 magnification, respectively. **f** The cross-sectional morphology of LSMO film on LAO

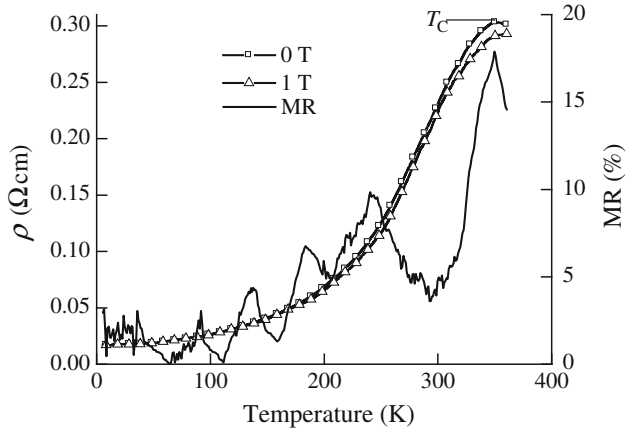

Fig. 4 Temperature dependence of resistivity for LSMO film on LAO (100) substrate. Solid lines are experimental data, and symbols represent the MR curve for LSMO film

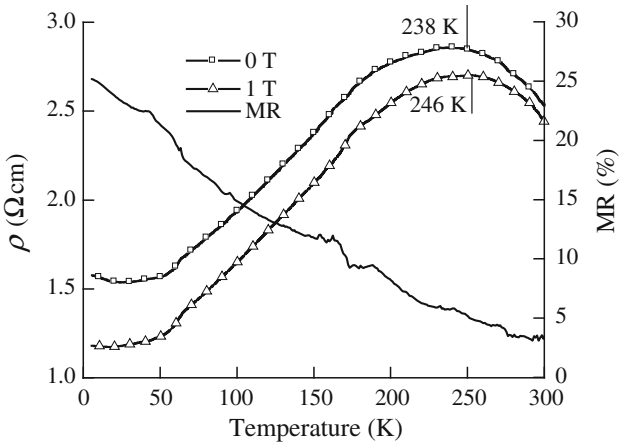

Fig. 5 Temperature dependence of resistivity for LSMO films on Si (100) substrate. Solid lines are experimental data, and symbols represent the MR curve for LSMO film

The resistance is reduced under applied magnetic field 1 T. Within double exchange model, the applied magnetic field can align these disordered spins between parallel arrangements Mn^{3+}−Mn^{4+} of LSMO, increase the transition probability of itinerant electrons, and reduce the spin disorder scattering; thereby the resistance is decreased effectively.

The curve of MR versus temperature is shown in Fig. 4, which has an obvious MR peak near T_C and the MR fluctuates in whole temperature range. The MR ratio here is illustrated as MR = $(\rho_0 - \rho_H)/\rho_0 \times 100$ %, where ρ_0 is the zero field resistivity and ρ_H is the resistivity in the applied field H. With decreasing temperature, MR shows an overall decrease with undulant pattern. The MR of the LSMO films on LAO mainly results from the suppression of spin fluctuation by magnetic field within grains and the contribution of the GBs to MR is inconsiderable [20]. The maximum value of MR is 2.67 % at 0.6 T (not shown here) and 5.17 % at 1 T when $T = 300$ K.

The temperature dependence of the resistance at different magnetic field (0 and 1 T) from 300 to 5 K and MR curve for LSMO films on Si are shown in Fig. 5. Compared with LSMO films on LAO, the transition temperatures of LSMO films on Si are lowered down to 238 K. Under the applied magnetic fields of 1 T, the resistance is remarkably suppressed in the wide temperature range and the T_{MI} shifts to a higher temperature (246 K), which is dominated by the spin-polarized tunneling at the GBs [21]. The external magnetic increases the carrier capacity and leads to a change in resistivity ρ. In addition, resistance gradually decreases at lower temperatures for LSMO films on LAO, but rises from 50 to 5 K for LSMO films on Si. The different transport behaviors are assumedly due to the magnetic domain walls at GBs and the reentrant effect in the polycrystalline films [20].

For the LSMO films on Si, the MR increases with decreasing temperature. It is suggested that magnetic external field prevents spin-dependent scattering of polarized electrons at the GBs and results in a large MR.

Obviously, the MR behavior of LSMO films on Si is different from LSMO films on LAO. A similar phenomenon was also observed by Liu et al. [22]. Single crystal and textured films have an MR peak in the vicinity of T_{MI}, while the polycrystalline LSMO films do not show the peak behavior. Thus, the crystalline orientation of the films plays an important role in governing the MR characterization.

4 Conclusions

Polycrystal LSMO thin films were synthesized on $LaAlO_3$ (100) and Si (100) single crystal substrates through spin-coating method by utilizing PACSD with PVP. XRD data shows evidence that the LSMO films on LAO is *a*—axis oriented and LSMO films on Si is polycrystalline, implying that the orientation of films depend on lattice mismatch degree between substrates and LSMO films. The resistance of LSMO films fabricated on $LaAlO_3$ substrates is smaller than that on the Si substrates. The magnetic field leads to reduced resistance of LSMO films both on LAO and Si in a wide temperature region, when the insulator-metal T_{MI} is shifted to a higher temperature. The LFMR of LSMO films on Si in low temperature range at 1 T is larger than that of LSMO films on LAO. The MR of LSMO films on LAO displays large values of MR as high as 5.17 % at room temperature. The MR of LSMO films on Si increases with decreasing temperature. The change in MR is related to GBs effect. Both films are smooth and dense with uniform nanocrystal size grain. The grain size of LSMO films on Si is larger than LSMO films on LAO. From the analysis, it is

found that crystalline orientation of substrates plays an important role in affecting grain size, structure, transport properties, and the MR characterization. These results demonstrate that PACSD is a viable method for growing high quality LSMO films.

Acknowledgments The research was supported by the Program of International S&T Cooperation 2013DFA51050, National Magnetic Confinement Fusion Science Program (2011GB112001), Science Foundation of Sichuan Province (2011JY0031, 2011JY0130), the financial support of the National Natural Science Foundation of China (No. 51271155, No. 51002125), and the Fundamental Research Funds for the Central Universities (SWJTU12CX018).

References

1. Urushibara A, Moritomo Y, Arima T et al (1995) Insulator-metal transition and giant magnetoresistance in $La_{1-x}Sr_xMnO_3$. Phys Rev B 51:14103–14109
2. Huang Y-H, Xu Z-G, Yan C-H et al (2000) Soft chemical synthesis and transport properties of $La_{0.7}Sr_{0.3}MnO_3$ granular perovskites. Solid State Commun 114:43–47
3. Rajeswari M, Shreekala R, Goyal A et al (1998) Correlation between magnetic homogeneity, oxygen content, and electrical and magnetic properties of perovskite manganite thin films. Appl Phys Lett 73:2634–2672
4. Thomas KA, de Silva PSIPN, Cohen LF et al (1998) Influence of strain and microstructure on magnetotransport in $La_{0.7}Ca_{0.3}MnO_3$ thin films. J Appl Phys 84:3939–3948
5. Lee KR, Chung YJ, Lee JH et al (2003) Electrical and magnetic properties of $La_{0.7}Ca_{0.3}MnO_3$ films prepared by RF magnetron sputtering method for colossal magnetoresistance applications. Thin Solid Films 426(1):205–210
6. Gao J, Shen SQ, Li TK et al (2003) Current-induced effect on the resistivity of epitaxial thin films of $La_{0.7}Ca_{0.3}MnO_3$ and $La_{0.85}Ba_{0.15}MnO_3$. Appl Phys Lett 82:4732–4734
7. Kang Y-M, Kim H-J, Yoo S-I et al (2009) Excellent low field magnetoresistance properties of the $La_{0.7}Sr_{0.3}Mn_{1+d}O_3$-manganese oxide composites. Appl Phys Lett 95:052510–052512
8. Viret M, Drouet M, Nassar J et al (1997) Low-field colossal magnetoresistance in manganite tunnel spin valves. Europhys Lett 39:545–549
9. Shim IB, Lee HM, Park KT et al (2002) Low-field magnetoresistance in sol–gel derived $La_{2/3}Sr_{1/3}MnO_{3-\delta}$ thick films. J Magn Magn Mater 242–245:1169–1171
10. Liu SM, Zhu XB, Yang J et al (2004) Fabrication of polycrystalline $La_{0.7}Sr_{0.3}MnO_3$ thin films on Si (1 0 0) substrates by chemical solution deposition. Phys B 353:238–241
11. Krishnan KM, Modak AR, Lucas CA et al (1996) Role of epitaxy and polycrystallinity in the magnetoresistance and magnetization of La0.8Sr0.2MnO3 thin films. J Appl Phys 79(8):5169–5171
12. Satoh I, Oniduka M, Kobayashi T (2002) PLD growth of $La_{0.7}Sr_{0.3}MnO_3$ tilted nanocolumn boundaries on constricted step-edged GaAs substrates and MR properties. Appl Surf Sci 197–198:527–531
13. Hawley MF, Adams CD, Arendt PN et al (1996) CMR films structure as a function of growth and processing. J Cryst Growth 174:455–463
14. Park S-I, Kim YH, Cho YS et al (2001) Characterization of La–Sr–Mn–O Films on Si(100) Grown by Using an rf–Sputtering Process under Different O_2 Partial Pressures. J Korean Phys Soc 38(1):38–41
15. Balevičius S, Cimmperman P, Petrauskas V et al (2005) Two phase structure of ultra-thin La–Sr–MnO films. Thin Solid Films 515:691–694
16. Toro RG, Fiorito DMR, Fragalà ME et al (2010) A novel MOCVD strategy for the fabrication of cathode in a solid oxide fuel cell: synthesis of $La_{0.8}Sr_{0.2}MnO_3$ films on YSZ electrolyte pellets. Mater Chem Phys 124:1015–1021
17. Méchin L, Adamo C, Wu S et al (2012) Epitaxial $La_{0.7}Sr_{0.3}MnO_3$ thin films grown on $SrTiO_3$ buffered silicon substrates by reactive molecular beam epitaxy. Phys Status Solidi A 209(6):1090–1095
18. Hasenkox U, Mitz C, Waser R (1999) Chemical Solution Deposition of Epitaxial $La_{1-x}(Ca, Sr)_x$ MnO_3.Thin Films. J Electroceram 3(3):255–260
19. Kartopu G, Yalçin O, Demiray AS et al (2011) Magnetic and transport properties of chemical solution deposited (100)—textured La0.7Sr0.3MnO3and La0.7Ca0.3MnO3 nanocrystalline thin films. Phys Scr 83:015701. doi:10.1088/0031-8949/83/01/015701
20. Yang SY, Kuang WL, Liou Y et al (2004) Growth and characterization of $La_{0.7}Sr_{0.3}MnO_3$ films on various substrates. J Magn Magn Mater 268:326–331
21. Chen Y, Wang G, Zhang S et al (2011) Magnetocapacitance effects of $Pb_{0.7}Sr_{0.3}TiO_3/La_{0.7}Sr_{0.3}MnO_3$ thin film on Si substrate. Appl Phys Lett 95:052910–052912
22. Liu SM, Zhu XB, Yang J et al (2006) The effect of grain boundary on the properties of $La_{0.7}Sr_{0.3}MnO_3$ thin films prepared by chemical solution deposition. Ceram Int 32:157–162